Proceedings of the ASME 2017 International Technical Conference and Exhibition on Packaging and Integration of Electronic and Photonic Microsystems
InterPACK2017
August 29-September 1, 2017, San Francisco, California, USA

IPACK2017-74132

INTEGRATED VAPOR CHAMBER HEAT SPREADER FOR POWER MODULE APPLICATIONS

Clayton L. Hose
Advanced Cooling Technologies, Inc.
1046 New Holland Avenue
Lancaster, PA, USA
clayton.hose@1-act.com

Dimeji Ibitayo
U.S. Army Research Laboratory
Sensors and Electron Devices Directorate
2800 Powder Mill Rd
Adelphi, MD, USA
oladimeji.o.ibitayo.civ@mail.mil

Lauren M. Boteler
U.S. Army Research Laboratory
Sensors and Electron Devices Directorate
2800 Powder Mill Rd
Adelphi, MD, USA
lauren.m.boteler.civ@mail.mil

Jens Weyant
Advanced Cooling Technologies, Inc.
1046 New Holland Avenue
Lancaster, PA, USA
jens.weyant@1-act.com

Bradley Richard
Advanced Cooling Technologies, Inc.
1046 New Holland Avenue
Lancaster, PA, USA
bradley.richard@1-act.com

ABSTRACT

This work presents a demonstration of a coefficient of thermal expansion (CTE) matched, high heat flux vapor chamber directly integrated onto the backside of a direct bond copper (DBC) substrate to improve heat spreading and reduce thermal resistance of power electronics modules. Typical vapor chambers are designed to operate at heat fluxes > 25 W/cm^2 with overall thermal resistances < 0.20 °C/W. Due to the rising demands for increased thermal performance in high power electronics modules, this vapor chamber has been designed as a passive, drop-in replacement for a standard heat spreader. In order to operate with device heat fluxes >500 W/cm^2 while maintaining low thermal resistance, a planar vapor chamber is positioned onto the backside of the power substrate, which incorporates a specially designed wick directly beneath the active heat dissipating components to balance liquid return and vapor mass flow. In addition to the high heat flux capability, the vapor chamber is designed to be CTE matched to reduce thermally induced stresses. Modeling results showed effective thermal conductivities of up to 950 W/m-K, which is 5 times better than standard copper-molybdenum (CuMo) heat spreaders. Experimental results show a 43°C reduction in device temperature compared to a standard solid CuMo heat spreader at a heat flux of 520 W/cm^2.

INTRODUCTION

There is a strong demand in the power electronics industry for modules with higher power densities and increased reliability [1-3]. Wide bandgap semiconductors (e.g. silicon carbide) are prime candidates for next-generation high-power switching for military, as well as commercial applications due to superior electrical, thermal, and mechanical properties compared to silicon (Si). For example, recent developments have given rise to silicon carbide (SiC) devices capable of power densities >500 W/cm^2 and maximum junction temperatures of 200°C. However, current state-of-the-art packaging is limited to heat dissipation of 200 W/cm^2 and 150°C. In order for SiC device technology to fully realize its potential, advanced packaging technologies need to be developed that are capable of handling the increased heat flux and higher temperatures.

A conventional power module is shown in Figure 1 and consists of power devices (Si and/or SiC) electrically connected by aluminum wire. The substrate is typically a direct bond copper (DBC) laminate with thick copper layers on both sides of a thick ceramic interlayer. The DBC is typically attached to a heat spreader (CuMo, CuW, or AlSiC) with solder, which is then attached to a heat sink with a thermal interface material (TIM). Power electronics packaging have many strict requirements including, but not limited to, high temperature and high frequency operation, high currents and voltages, large thermal and power cycles, and harsh operating environments.

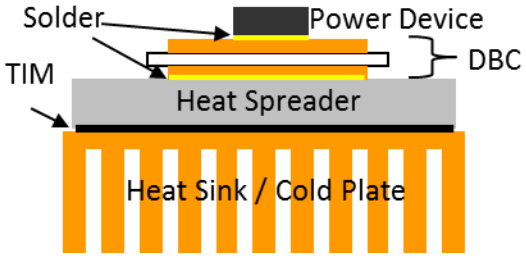

Figure 1. Conventional power module.

As power modules continue to decrease in size while increasing in power capabilities, advanced thermal solutions are required to dissipate the increased amounts of waste heat. Increasing the ability to spread heat from a concentrated heat input area (device scale) to a larger heat dissipation area (heat sink) has the potential to significantly reduce the maximum temperature a device reaches during operation. Current power electronics packaging often limits the ability to realize the full potential of advanced power electronics diodes and MOSFETs, thus requiring them to be derated. The ability to more effectively remove the heat from the device allows a more reliable module that can operate closer to its rated conditions, and can reduce system size and weight.

Conductive heat spreading is limited by the thermal conductivity and thickness of the spreader. When conductive heat spreaders fail to achieve acceptable operating temperatures, vapor chambers are commonly used to greatly improve heat spreading. A vapor chamber operates using the latent heat of vaporization of a working fluid to transport heat using pressure differentials to flow the working fluid in a cycle from a heat input area to a heat output area and back. Figure 2 illustrates the operating principle of a vapor chamber. Vapor chamber performance limits are dictated by several fluid flow related limitations, primarily liquid working fluid return flow. This work focuses on utilizing advanced heat spreader technology previously developed and demonstrated by the author's employer [4] to design, development, and demonstration a CTE matched, high heat flux vapor chamber heat spreader to show a path toward a substantial improvement in waste heat removal and power module reliability. This is a CTE matched, passive packaging solution with built-in electrical isolation and the ability to act as a drop-in replacement for the current heat spreader.

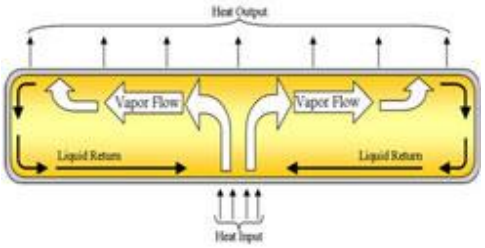

Figure 2. Conceptual operation of a vapor chamber.

BACKGROUND

Advanced vapor chambers designed to dissipate heat in high flux regions have been built and tested in a laboratory environment achieving heat fluxes in excess of 700 W/cm^2 [5,6]. These vapor chambers were designed using CTE matched materials targeting direct die attachment. Specialized wick features within the vapor chamber allow the working fluid within the vapor chamber to vaporize and flow more readily than standard vapor chamber designs [4].

The vapor chamber working fluid plays a considerable role in the heat transport capabilities of a vapor chamber. The two-phase operating principle of a vapor chamber uses the latent heat of vaporization of the working fluid to transport heat in the vapor phase of the working fluid. Since each fluid has a different latent heat of vaporization, as well as other thermodynamic properties, working fluid selection is critical for optimum vapor chamber operation. A quantitative method of comparing working fluids is a figure of merit as shown in Eq. 1 [7], which relates important working fluid properties that play a role in working fluid flow and thermal energy storage. Figure 3 shows working fluid figure of merit for a large number of working fluids typically used in passive two-phase heat transfer devices, such as vapor chambers and heat pipes.

$$N_l = \frac{\rho_l \sigma \lambda}{\mu_l} \quad (1)$$

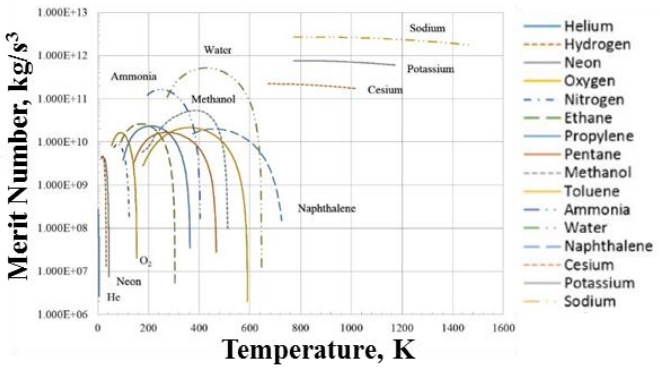

Figure 3. Figure of merit for commonly used working fluids of passive heat transfer devices.

It is evident from Figure 3, water is an ideal working fluid for operation between 20 and 300+°C; however, it is worth noting the vapor pressure of the working fluid is not captured in the figure of merit, but play an important role in the design of a

vapor chamber. A vapor chamber's internal operating pressure is dictated by the saturation curve of the working fluid since the vapor chamber is evacuated then charged with the working fluid to eliminate non-condensable gases that would interfere with the operation of the vapor chamber. For water, operation above 100°C generates internal pressures greater than atmospheric pressure. A positive internal pressure differential requires special considerations in the design of the vapor chamber envelope/structure. Vapor chambers utilizing water as the working fluid have been developed to operate above 100°C with specialized structural supports [8], but are not implemented into the work presented here.

FABRICATION

One requirement of the replacement vapor chamber heat spreader is to be a drop in replacement for the CuMo heat spreader of the power module currently under consideration. The CuMo heat spreader is 2.5 inches in width, 2.0 inches in depth, and .157 inches thick. The DBC substrate is 1.65 inches in width, 1.73 inches in depth, and .049 inches thick (.025 inch thick aluminum nitride with, .012 inch thick copper layers on both sides). The three electrical devices each have a contact area .159 inches in width and .258 inches in depth. Figure 4 shows the 3D solid model of the high heat flux vapor chamber heat spreader with integral DBC substrate and electrical devices attached.

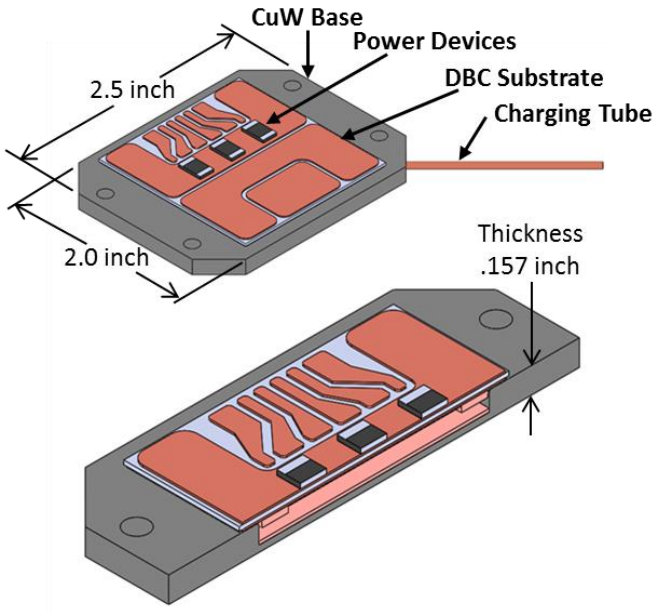

Figure 4. 3D solid model of high heat flux vapor chamber heat spreader (top) and cross-section of high heat flux vapor chamber heat spreader (bottom).

The vapor chamber heat spreader was designed with a copper-tungsten (CuW) metal matrix composite single piece base onto which the DBC substrate is brazed. The base and DBC substrate have a copper powder wick attached prior to assembly to facilitate liquid working fluid flow to the heat input area. The porous structure of the wick and surface tension of the working fluid (water) generate capillary pressure which acts to "pump" the condensed working fluid back to the area opposite to the heat input where the working fluid is vaporized. The areas of wick opposite to the heat input areas have converging lateral arteries developed by the author's employer to accommodate the high input heat flux [4]. Figure 5(a) and (b) show trial vapor chamber components with attached wicks. Figure 5(c) shows the converging lateral arteries of a high heat flux vapor chamber wick. Bonding between the CuW base and DBC/wick was facilitated by metalizing the CuW base with copper. This metallization also provides a barrier between the working fluid and base material. The working fluid and the materials wetted by the working fluid must be compatible in that they must not generate gases when in contact with each other under vacuum. If non-condensable gases are generated inside a vapor chamber, internal areas of the vapor chamber will be blocked by the gas causing these areas to not participate appreciably in heat transfer. Copper and water are known to be compatible as their use in heat pipes is extensively documented [7]; however, insufficient compatibility data is currently available between water and tungsten. Working fluid feeder structures are formed integral to the wick to facilitate liquid working fluid flow from the CuW base wick where the working fluid condenses to the converging lateral arteries in the DBC wick where the working fluid evaporates. Contact between the wicks is facilitated by layers of copper screen captured between CuW base wick and feeder features on the DBC wick prior to assembly of the two components. The CuW base also includes a central structural post to limit DBC deflection when the vapor chamber is evacuated and operating below 100°C. A charging tube was also brazed into the vapor chamber base for evacuation and fluid charging. Once assembled, the vapor chamber had the electronic devices attached using high-temperature solder. With the devices attached, the vapor chamber was charged with the appropriate volume of water. Figure 5 (d) shows the assembled CTE matched, high heat flux vapor chamber heat spreader.

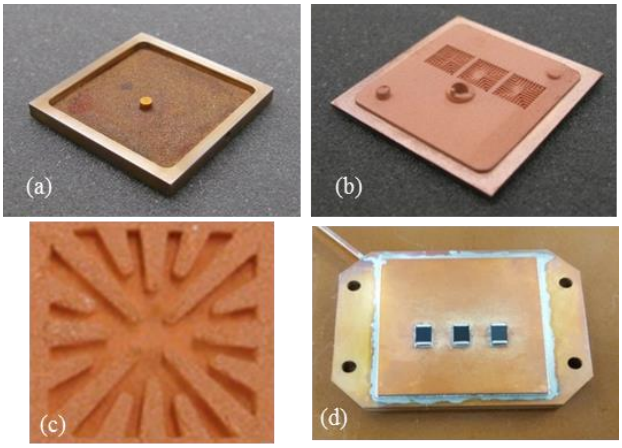

Figure 5. (a) Copper plated trial CuW base with copper wick, (b) DBC with copper wick including high heat flux provisions, (c) converging lateral arteries of the high heat flux wick region, and (d) completed CTE matched, high heat flux vapor chamber heat spreader.

EXPERIMENTAL RESULTS

An experimental setup was developed in order to investigate the performance of the vapor chamber heat spreader compared to a standard CuMo heat spreader. The set up consisted of a DC power supply, liquid-cooled heatsink, chiller, flow meter, flow valve and an infrared (IR) camera.

The heat spreaders were mounted on a D6 Industries liquid-cooled heatsink using an Arctic Silver thermal adhesive compound. A Julabo recirculating chiller was used to supply water through the heat sink at an inlet temperature of 30°C. The heatsink outlet temperature was measured using a thermocouple. The flow rate used for testing was ~0.85 gpm.

A 0-90 V, 0-8 A DC power supply was used to apply power to 0.25 cm^2 ceramic chip resistors mounted on the heat spreaders. The maximum power during testing was limited by the temperature limits of the chip resistor and device attach material. Prior to testing, the top surfaces of the modules were coated with boron nitride spray in order to provide uniform surface emissivity for IR imaging [9]. Figure 6 shows the vapor module mounted inside the test bed with several coats of boron nitride applied. A FLIR A40 IR camera and associated software was used to measure the surface temperature of the device as well as several surrounding locations to further evaluate heat spreading performance for each module. After thermal equilibrium was achieved at each power level, the resistor temperature was recorded using the IR camera software. The heatsink outlet temperature was also recorded.

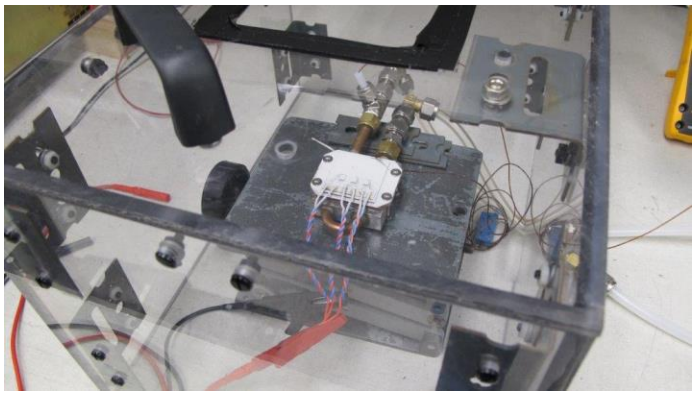

Figure 6. Vapor chamber heat spreader mounted on liquid-cooled heatsink for testing.

The CuMo heat spreader resistor was tested to a maximum of 130 W (~ 520 W/cm^2) and the resistor on the vapor chamber heat spreader was tested up to 148 W (~ 600 W/cm^2). The reduction in device temperature with the vapor chamber versus the CuMo heat spreader made it possible to test the vapor chamber heat spreader at an additional power level while maintaining a safe operating temperature. Figure 7 compares the temperature rise of the resistor in both heat spreaders. This plot shows that the performance of the vapor chamber heat spreader over the CuMo heat spreader becomes more and more pronounced with increasing heat flux. Figure 8 shows infrared images for both heat spreaders with the test resistor in each case operating at ~ 520 W/cm^2. The measured average rise in device temperature of the vapor chamber device was 50 degrees lower than the CuMo resistor at this same heat flux. Figure 8 also illustrates the superior heat spreading performance of the vapor chamber heat spreader.

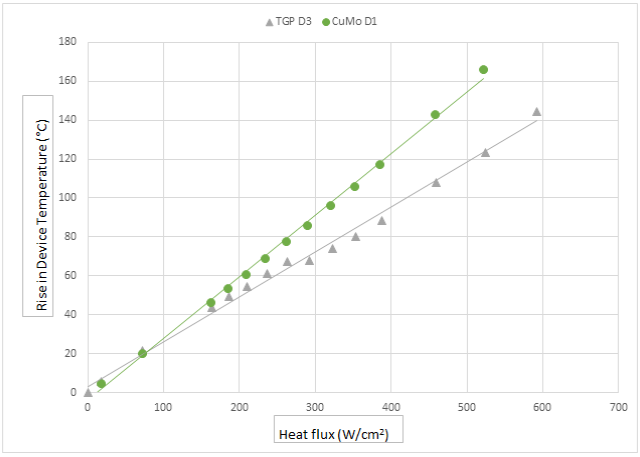

Figure 7. Comparison of the rise in chip resistor temperature for CuMo versus vapor chamber heat spreader over a range of heat fluxes.

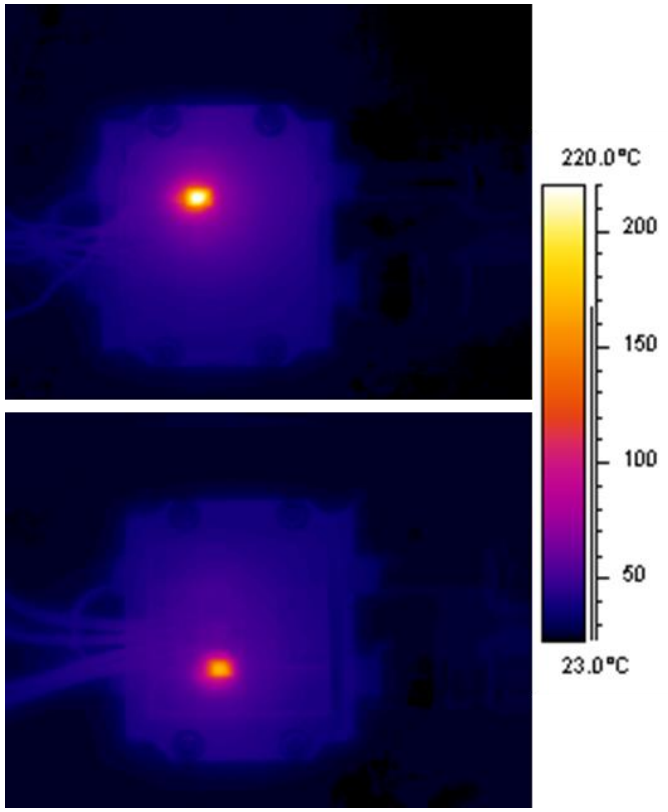

Figure 8. Infrared images of CuMo (top) and vapor chamber (bottom) heat spreaders.

MODELING RESULTS

In order to quantify the performance improvement through the implementation of a vapor chamber heat spreader, a finite element analysis (FEA) using ANSYS was performed comparing the standard CuMo heat spreader to the advanced vapor chamber heat spreader. Initially, an FEA analysis was performed to determine the effective heat transfer coefficient induced by the heat sink. The comparison was made by changing the heat transfer coefficient until it closely matched the experiment over a wide range of heat fluxes. After a series of iterations, it was determined the heat sink has a heat transfer coefficient to be 1275 W/m^{2}K. The comparison of the FEA to the experiment for the CuMo heat spreader is shown in Figure 9 which is a plot of the maximum chip temperatures for both the FEA and experiment. The maximum temperature difference is <9°C and occurs at the highest heat flux, all other temperatures were within 2 degrees.

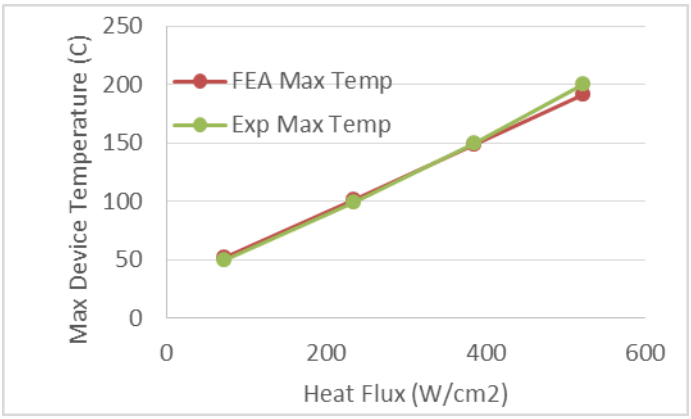

Figure 9. Finite element analysis versus experimental results for copper-molybdenum heat spreader.

Next this heat transfer coefficient was used to determine the effective thermal conductivity of the vapor chamber heat spreader. This was done by placing the determined heat transfer coefficient (1275 W/m^2-K) on the backside of the heat spreader and then varying the thermal conductivity of the vapor chamber heat spreader until it matched the experiment. The results are shown in Figure 10 plotted against both heat flux and maximum chip temperature. The results show an effective thermal conductivity that peaks at 950 W/m-K, which occurs at a heat flux of 354 W/cm^2 and a maximum chip temperature of 112°C. This thermal conductivity is about 5 times better than standard heat spreader materials (CuMo, CuW, or AlSiC) and about 2.5 times better than copper.

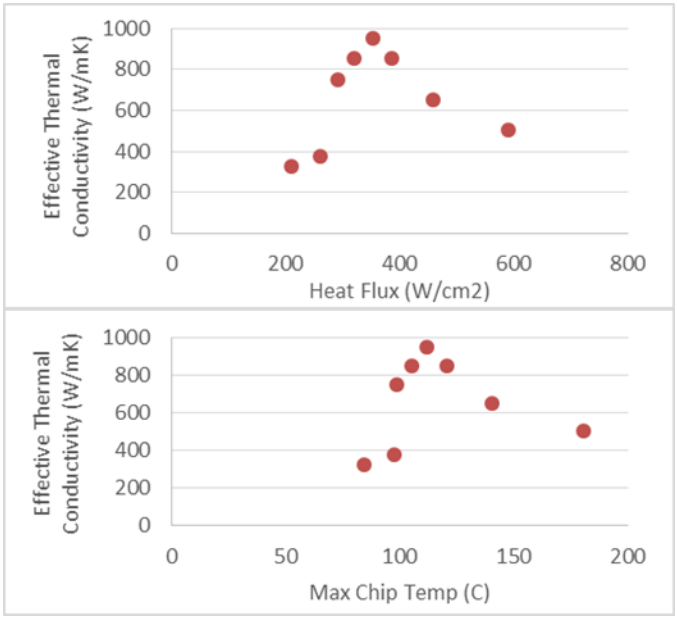

Figure 10. Vapor chamber heat spreader effective thermal conductivity as a function of heat flux (top) and maximum chip temperature (bottom).

Figure 11 shows the FEA solutions that correspond to the IR images from Figure 8 at a heat flux of 520 W/cm^2. These results also show the difference in temperature and the increased temperature uniformity for the vapor chamber heat spreader over the standard CuMo heat spreader.

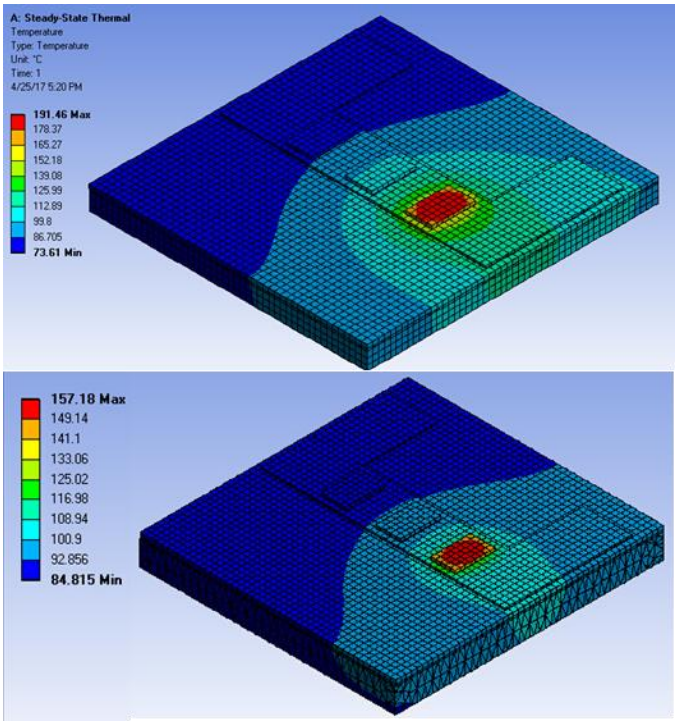

Figure 11. FEA solutions corresponding to Figure 8 infrared images of copper-molybdenum (top) and vapor chamber (bottom) heat spreaders.

CONCLUSIONS

A CTE matched, high heat flux vapor chamber has been developed to meet the rising demands of power density and reliability in power electronics. The vapor chamber utilizes components that are well matched to the envelope material to reduce stress and improve reliability. The high heat flux handling capability of the vapor chamber heat spreader is made possible by the integration of a special wick structure beneath the critical heat flux areas (i.e. resistors for this work). Modeling results showed between a 2-5x increase in heat spreader thermal conductivity over a wide range of heat fluxes and operating temperatures. This paper has experimentally demonstrated the ability to replace an existing CuMo heat spreader with a passive drop-in replacement vapor chamber resulting in significant temperature reduction of 43°C at a heat flux of 520 W/cm^2.

ACKNOWLEDGMENTS

The authors would like to thank Charles Scozzie, Damian Urciuoli, Nicholas Jankowski, Darin Sharar, Claude Pullen, Michael Rego, Morris Berman, Bruce Geil, and Michael Ames for their valuable contribution to this work. This research was sponsored by the U.S. Army Research Laboratory and was accomplished under Cooperative Agreement Number W911NF-16-2-0047.

NOMENCLATURE

N –figure of merit
ρ – density
σ – surface tension
λ – latent heat of vaporization
μ – dynamic viscosity

Subscript

l – liquid phase

REFERENCES

[1] Park, C.; Jaura, A. K. Thermal Analysis of Cooling System in Hybrid Electric Vehicles. SAE Transactions, SAE-2002-01-0710.

[2] Kuszewski, M.; Zerby, M. Next generation Navy thermal management program. CARDIVNSWC-TR-82-2002/12, 2002.

[3] Ponnappan, R.; Donovan, B.; Chow, L. High power thermal management issues in space-based systems. Space Technology and Applications International Forum-STAIF 2002, Albuquerque, New Mexico, February 3–6, 2002.

[4] Ju, Y.S., Kaviany, M., Nam, Y., Sharratt, S., Hwang, G.S., Catton, I., Fleming, E., and Dussinger, P., 2013, "Planar vapor chamber with hybrid evaporator wicks for the thermal management of high-heat-flux and high-power optoelectronic devices," Int. J. Heat Mass Transfer, 60(1), pp. 163-169.

[5] Kristen P. Bloschock ; Avram Bar-Cohen; Advanced thermal management technologies for defense electronics. Proc. SPIE 8405, Defense Transformation and Net-Centric Systems 2012, 84050I (May 3, 2012); doi:10.1117/12.924349.

[6] A. Bar-Cohen, K. Matin, N.R. Jankowski, and D.J. Sharar, 2014, "Two-phase thermal ground planes: technology development and parametric results," ASME Journal of Electronic Packaging, 137 (1).

[7] Kew, P. A., and Reay, D. A., 2006, *Heat Pipes*, Butterworth-Heinemann, Oxford.

[8] Pounds, D.A., and Bonner II, R.W., "Vapor Chamber Structure," U.S. Patent 9,204,574 B1, Dec. 1, 2015.

[9] Salem, T.E., Ibitayo, D., Geil, B.R., "Validation of Infrared Camera Thermal Measurements on High-Voltage Power Electronic Components", IEEE Transactions on Instrumentation and Measurement 56(5), 2007.